Kinetics of the premelting ($L_{\beta'}$-$P_{\beta'}$) and main transition ($P_{\beta'}$-L_α) in hydrated dipalmitoylphosphatidylcholine

A time-resolved x-ray diffraction study using microwave-induced temperature-jumps

Martin Caffrey,* Gary Fanger,* Richard L. Magin,‡ and Jian Zhang‡

*Department of Chemistry, The Ohio State University, Columbus, Ohio 43210 and ‡Bioaccoustic Research Laboratory, University of Illinois, Urbana, Illinois 61801 USA

ABSTRACT The dynamics and mechanism of the premelting ($L_{\beta'}$-$P_{\beta'}$) and main transitions ($P_{\beta'}$-L_α) in fully hydrated dipalmitoylphosphatidylcholine were examined by low-angle time-resolved x-ray diffraction (TRXRD) using microwave radiation to effect uniform, internal sample heating. Equilibrium and dynamic aspects of the transitions were investigated. The dynamic studies involved applying a temperature jump of sufficient amplitude to effect the two transitions sequentially. Our findings are as follows. (*a*) Microwave radiation has proven useful as a means for implementing rapid and uniform internal heating in temperature-jump studies of lipid-phase transition kinetics. (*b*) Heating rate can be controlled by adjusting microwave power setting. (*c*) The thermal expansion coefficient of the three lyotropic phases follows the sequence $L_{\beta'} \doteq O > P_{\beta'} \gg L_\alpha$. (*d*) Regardless of temperature-jump amplitude and sample heating rate the $P_{\beta'}$ phase was always in evidence as an intermediate between the $L_{\beta'}$ and L_α phases. (*e*) The degree of development of the $P_{\beta'}$ phase was inversely proportional to temperature-jump amplitude and heating rate. (*f*) The shortest transit time recorded for the combined $L_{\beta'}$-$P_{\beta'}$, and $P_{\beta'}$-L_α transitions was <1 s. (*g*) Upon cooling from the L_α phase the onset of the chain disorder/order transition was apparent as a dramatic change of slope in the scattering angle vs. time plot which is interpreted as arising from sample heating by the latent heat of the transition. (*h*) Based on the shape of the low-angle diffraction pattern of the $P_{\beta'}$ phase the $P_{\beta'}$-L_α transition appears to be reversible with no evidence of metastability as was observed in the *slow scan* TRXRD measurements of Tenchov et al. (1989. *Biophys. J.* 56:757–768).

INTRODUCTION

Under conditions of full hydration the thermotropic phase sequence observed with the saturated, homoacid phosphatidylcholines (PC)[1] is subgel, lamellar gel ($L_{\beta'}$), ripple ($P_{\beta'}$), and lamellar liquid crystalline (L_α; Small, 1987). The $P_{\beta'}$ phase appears as an intermediate between the $L_{\beta'}$ and L_α phases. The kinetics of its formation upon heating from $L_{\beta'}$ and cooling from the L_α phase has been studied by a variety of techniques (Blume and Hillman, 1986; Cho et al., 1981; Genz and Holzwarth, 1986; Genz et al., 1986; Inoue et al., 1981, 1985; Johnson et al., 1983; Lentz et al., 1978; Mayorga et al., 1988; Subczynski and Kusumi, 1986; Teissie et al., 1979; Tsong, 1974; Tsong and Kanehisa, 1977; Tsuchida et al., 1985; see Caffrey, 1989*a*, *b* for a review of kinetic x-ray studies of transitions involving the $P_{\beta'}$ phase). Recent slow-scan, time-resolved x-ray diffraction (TRXRD) work shows that in the case of fully hydrated dipalmitoylphosphatidylcholine (DPPC) the $P_{\beta'}$ phase forms relatively rapidly in the heating direction but that a metastable (mst) form of $P_{\beta'}$, identified as $P_{\beta'}$ (mst), emerges upon cooling from the L_α phase (Tenchov et al., 1989). Reformation of the original $P_{\beta'}$ phase is achieved only by first cooling $P_{\beta'}$ (mst) into the $L_{\beta'}$ phase. Prolonged incubation in the $P_{\beta'}$ (mst) phase for up to 24 h does not facilitate conversion to the original $P_{\beta'}$ phase.

Our research program concerns the study of the kinetics and mechanism of lipid phase transitions using TRXRD (Caffrey, 1984*a*, 1987, 1989*a*). We have long been interested in the $P_{\beta'}$ phase because it is a phase which is periodic in two dimensions and appears in the thermotropic and barotropic sequence as an intermediate between the $L_{\beta'}$ and L_α phases (Shashidar et al., 1984), both of which are periodic in one dimension. In an effort to gain insights into the mechanism of these phase interconversions which involve quite dramatic structural rearrangements and changes in hydration levels we set about studying the phase sequence, $L_{\beta'}$-$P_{\beta'}$-L_α, using TRXRD in conjunction with a temperature-jump perturbation. The question posed concerned the possible elimination or bypassing of the $P_{\beta'}$ phase as an intermediate phase in the above sequence as the sample heating rate was increased. Our results show that for heating rates up to 29° C/s the $P_{\beta'}$ phase *always* appears as an intermediate. The second

[1] *Abbreviations used in this paper:* CHESS, Cornell High Energy Synchrotron Source; DPPC, dipalmitoylphosphatidylcholine; Hepes, 4-(2-hydroxyethyl)-1-piperazineethane-sulfonic acid; L_α, lamellar liquid crystal phase (the lipid phase notation used is that of Luzzati, 1968); $L_{\beta'}$, lamellar gel phase; (mst), metastable; MED, microwave exposure device, $P_{\beta'}$, ripple phase; PC, phosphatidylcholine; TRXRD, time-resolved x-ray diffraction.

0006-3495/90/09/677/10 $2.00

question concerned the nature of the $P_{\beta'}$ phase obtained upon cooling from L_α. The TRXRD data show that $P_{\beta'}$ so obtained is not of the metastable kind described by Tenchov et al. (1989). In fact, the low-angle diffraction pattern of the $P_{\beta'}$ phase obtained upon heating from $L_{\beta'}$ and cooling from L_α are virtually identical for the particular set of conditions used in these experiments.

MATERIALS AND METHODS

Materials

DPPC, obtained from Avanti Polar Lipids, Inc. (Birmingham, AL), was used as purchased. Previous studies had shown this material to be of consistently high purity (≥98% based on thin layer chromatography as described by Caffrey and Feigenson, 1981). Water was obtained from a Milli-Q water purification system (Millipore Corp., Bedford, MA). All other solvents and chemicals were of reagent grade.

Sample preparation

Fully hydrated samples of DPPC in thin-walled (10-μm) glass or quartz capillaries (1-mm internal diam; Charles Supper Co., Natick, MA) were prepared in excess 10 mM Hepes, 0.14 M NaCl, 7 mM KCl, pH 7.4 as previously described (Caffrey and Feigenson, 1984) with the exception that the capillaries were left unsealed to provide access for the microwave compatible temperature sensor (Luxtron Type LIA, Luxtron Corp., Santa Clara, CA). The sensor, connected to a model 2000 fluoroptic thermometer (Luxtron Corporation), consisted of a 1-mm diam optical fiber with a temperature-sensitive mixture of rare earth phosphors deposited in a thin layer at its tip (Wickersheim and Alves, 1979). The sensor tip was immersed in the DPPC/water sample as close to the position of the x-ray beam as possible. However, due to variability in the capillary bore along its length, the relative position of sensor and x-ray beam varies between samples. At no time was the sensor sealed in the capillary.

X-Ray diffraction

X-Ray diffraction measurements were carried out by using wiggler-enhanced, monochromatic (0.157 nm), focused x-rays on the A1 line at the Cornell High Energy Synchrotron Source (CHESS) as previously described (Caffrey, 1987). The machine was operating at 5.2 GeV and 20–50 mA total electron beam current in the seven-bunch mode and with the six pole wiggler at half power. X-Ray exposure of the sample was kept to a minimum throughout the measurements by judicious use of a beam shutter. Because of limitations in the design of the microwave exposure device, it was not possible to translate and rotate the sample continuously during the measurements to further reduce radiation damage effects (Caffrey, 1984*b*, 1989*a*).

Static and time-resolved x-ray diffraction measurements were made using a homebuilt, low-angle x-ray diffraction camera as previously described (Caffrey et al., 1990). The camera incorporates an optical bench, 0.3-mm diam collimator (Charles Supper Co.), beam stop, film cassette, and an x-ray imaging and recording device. The latter consists of a three-stage image intensifier tube and a video camera fitted with an f0.85, 25-mm lens. The enhanced x-ray image from the intensifier was viewed via the camera using a front-surfaced mirror positioned at a 45° angle with respect to the optical axis of the intensifier and the camera.

Static x-ray diffraction patterns were recorded on x-ray sensitive film (CEA Reflex 25; CEA America Corp., Greenwich, CT; DEF5; Kodak, Rochester, NY) and the x-ray wavelength (1.565 Å) was determined using a lead nitrate standard as previously described (Caffrey, 1987).

A complete description and the performance characteristics of the system for making TRXRD measurements have been reported (Caffrey, 1987 and references therein). The essential components are an x-ray camera (described above), a two-dimensional, live-time x-ray imaging device, a character generator, an electronic clock, a frame counter, and a video camera, recorder, and monitor. Quantitative diffracted intensity and position information was obtained by digital processing the live-time diffraction images recorded on video tape. Except for frame and/or circular averaging, the raw, uncorrected data are presented in this communication.

Data analysis

The video recorded data is quantitated by digital image processing (Trapix 55/48; Recognition Concepts, Inc., Carson City, NV) using a combination of commercial (RTIPS; Tau Corp., Dayton, OH) and home-written software. Sequential digitized images or parts thereof are "grabbed" and stored in the memory of the image processor. Preliminary processing such as frame and/or circular averaging is performed on the image processor under microcomputer control. The data is then ported to a Macintosh II computer where it is further processed to locate diffracted peak maxima (Mencke and Caffrey, manuscript submitted for publication). Because of jitter in the original taped material pixel position has an associated error of ±1 pixel.

Microwave exposure device (MED)

The MED consists of a hollow rectangular piece of aluminum waveguide (WR-284) with internal dimensions of 43.2 cm × 7.2 cm × 3.4 cm and with a wall thickness of 2 mm. The waveguide section was modified to provide an access and positioning port for the sample. For this purpose 3-mm diam holes were drilled and tapped on the top and bottom of the waveguide. In the holes were threaded hollow teflon inserts that provided vertical support and positioning of the x-ray capillary to within ± 2 mm of the center of the waveguide. In addition, holes of 1-mm and 2.8-cm diam were machined through the side walls of the waveguide to accommodate the incident and diffracted x-ray beams. To maintain electrical continuity of the waveguide sidewalls, the exit port was covered with 25-μm thick aluminum foil. This ensures the flow of surface currents because the skin depth in aluminum for the penetration of an electric field at 2.45 GHz is ~1 μm. A complete description of the MED and its performance characteristics has been presented (Caffrey et al., 1990).

Experiments were performed by recording the live-time x-ray diffraction image initially in the absence of microwave radiation to obtain a baseline ambient temperature pattern. Microwave power was then set to the desired level and the changing diffraction pattern was recorded usually until a stable final sample temperature was reached. Heating was terminated by turning off the microwave power and allowing the sample to cool passively in air. Again, the live-time x-ray diffraction pattern was recorded as the sample cooled. Sample heating and cooling profiles in the MED have been described previously for a lipid/water system similar to the one used in these experiments (Caffrey et al., 1990). Theory and experiment show heating rates of ~0.4° C/s. W for pure water samples in a similar experimental configuraion. A 5-W temperature jump provided an average heating and an initial cooling rate of 1.0 and 2.8° C/s (Fig. 3 in Caffrey et al., 1990).

Thermal equilibrium measurements were performed by setting micro-

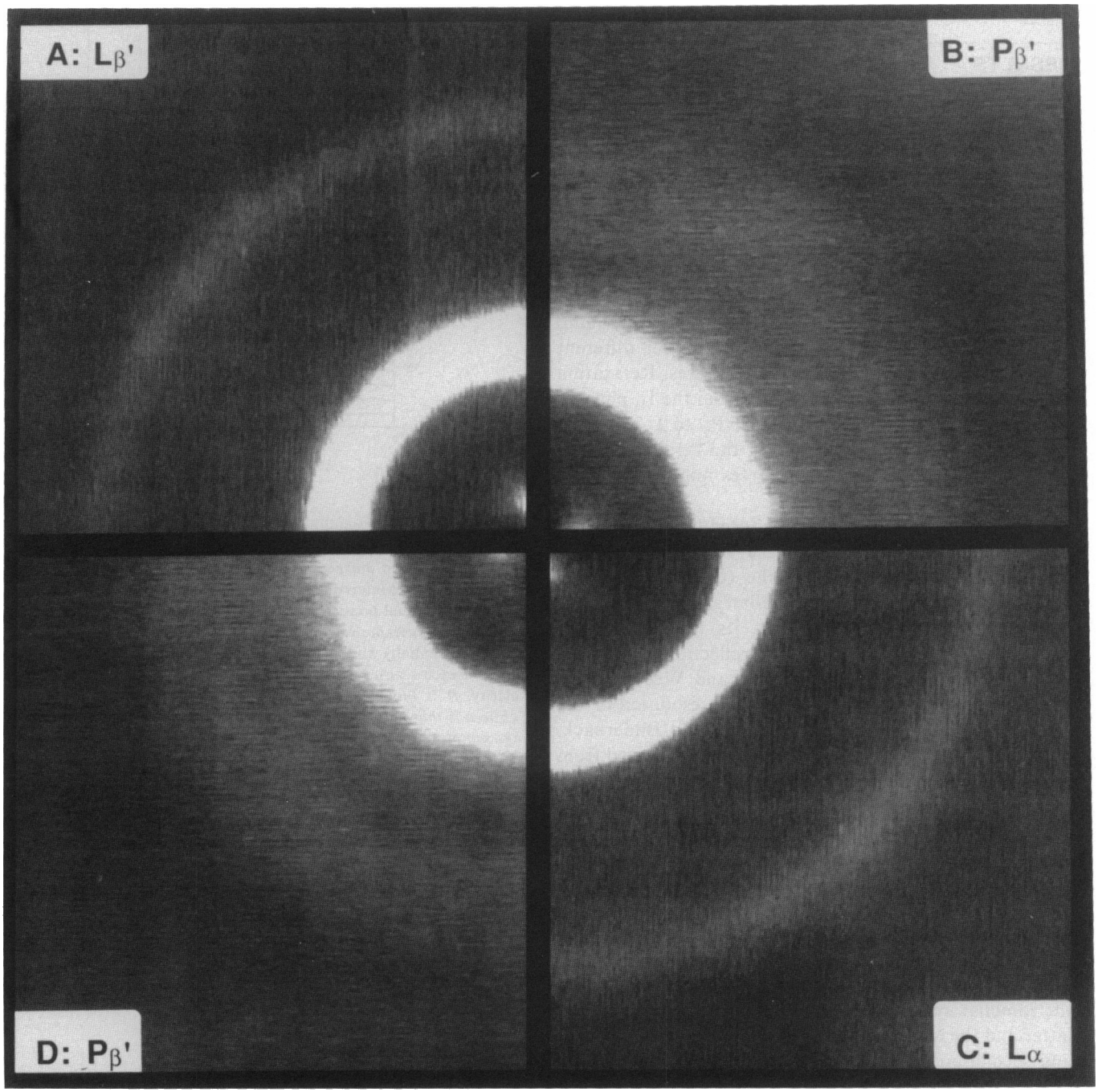

FIGURE 1 Low-angle time-resolved x-ray diffraction images of the $L_{\beta'}$, $P_{\beta'}$, and L_{α} phases in fully hydrated DPPC. Each sector in the composite corresponds to part of a single (33 ms) video frame and was obtained by digitizing the original video images recorded in live time. Images *A–C* were recorded in the heating direction. Image *D* corresponds to the $P_{\beta'}$ phase obtained upon cooling from the L_{α} phase. Heating was effected by microwave irradiation.

wave power to a given level and allowing the sample to reach thermal equilibrium (usually within 2 min) before recording the diffraction pattern.

RESULTS

We present our results in two parts. The first concerns equilibrium measurements wherein low-angle TRXRD data were collected at a series of fixed temperatures in the range which encompasses all three phases. These equilibrium measurements serve as a reference with which the dynamic data will be compared. The second part of the results section addresses the dynamic measurements wherein the change in the low-angle diffraction pattern is monitored continuously in time after a temperature jump of varying amplitude. The latter provides for different heating rates and final sample temperatures. Relaxation back into the $P_{\beta'}$ phase upon cooling from the L_α phase is also described. The conversion from $P_{\beta'}$ to $L_{\beta'}$ was not monitored in this study because of the tardiness of the transition. Conventional x-ray sources might be used to advantage in such a study.

The various transitions are monitored by following the position in reciprocal space of the strongest low-angle reflection. This corresponds to the (0, 0, 1) and (1, 0) reflections in the case of the lamellar and ripple phases, respectively. The $P_{\beta'}$ phase, with its two-dimensional periodicity, has additional satellite reflections (Janiak et al., 1976; Inoko et al., 1980; Wack and Webb, 1989). Because of the less than ideal angular resolution of the present x-ray imaging system (Caffrey and Bilderback, 1984) the weak (1, 1) reflection is not fully resolved from the (1, 0) lamellar reflection and appears as a shoulder on the wide-angle side of the latter. The low-angle (0, 1) reflection is masked by the beam stop. Furthermore, the other considerably weaker (0, 3), (0, 4), and (1, 3) reflections intervening between the (1, 0) and (2, 0) lines contribute to increased scattering in this region. The most notable features of the low-angle diffraction pattern of the $P_{\beta'}$ phase, which serve to distinguish it from the two other phases, are the dramatic decrease in scattering angle of the lamellar reflection, the apparent asymmetry of the latter and the enhanced scattering level between the first- and second-order lamellar reflection (see Figs. 1 and 2 below). We use these characteristics as criteria for the development of the $P_{\beta'}$ phase in the course of the dynamic heating and cooling experiments.

Throughout this study we have used microwave radiation to effect rapid and uniform internal sample heating. One difficulty associated with the use of microwaves concerns the accurate determination of in-sample temperature while the sample is being irradiated. This requires the use of expensive, microwave-compatible temperature sensors. In this work we were unable to make accurate in-sample temperature measurements because of the limited range of sensor sizes available at the time. *We are careful to note, therefore, that all temperatures reported in this paper are nominal.* Despite this immediate shortcoming the results demonstrate the utility of employing microwave radiation in studies of this type.

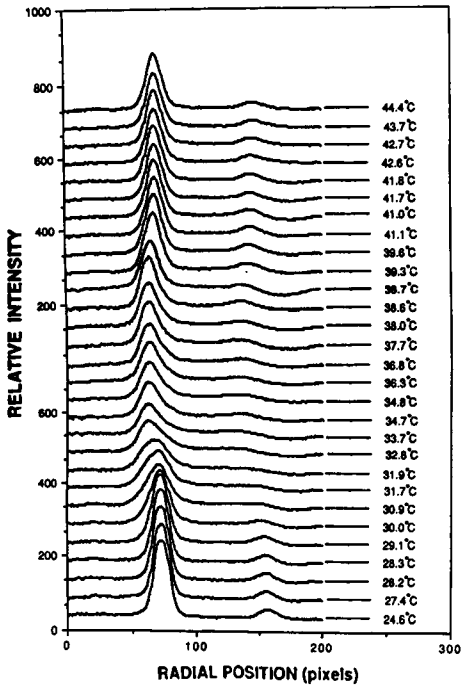

FIGURE 2 Thermal equilibrium measurements of the microwave-induced $L_{\beta'}$-$P_{\beta'}$-L_α phase transition sequence occurring in fully hydrated DPPC. Low-angle diffraction data were recorded using TRXRD as described under Materials and Methods. Each scan corresponds to an intensity vs. radial position (I-2θ) plot obtained by image processing a single (33 ms) frame with radial averaging over a 20° arc. Scans are shown sequentially with increasing sensor temperature (indicated to the right of each scan). Scans are displaced vertically on the ordinate for clarity. *It is important to note that the temperature shown on the absicca is that recorded at the sensor and is not that at the position in the sample of the interrogating x-ray beam.*

Equilibrium measurements

The low-angle diffraction patterns recorded by TRXRD in the $L_{\beta'}$, $P_{\beta'}$, and L_α phases upon heating and the $P_{\beta'}$ phase upon cooling from the L_α phase are shown in Fig. 1. The patterns were recorded after equilibrating the sample for 1–2 min at each temperature. In Figs. 1, *A* and *C* the (001) and (002) lamellar reflections are clearly visible. The diffraction pattern typical of the $P_{\beta'}$ phase obtained upon heating from the $L_{\beta'}$ phase (Fig. 1 *B*) and upon cooling from the L_α phase (Fig. 1 *D*) is also shown.

The intensity vs. scattering angle (I-2θ) scans recorded at a series of temperatures encompassing the $L_{\beta'}$, $P_{\beta'}$, and L_α phases upon microwave heating are shown in Fig. 2. The corresponding sensor temperatures are shown to the right hand side of each scan. We emphasize that these are *nominal temperatures* and are not necessarily the actual temperatures at the interrogation site of the x-ray beam in the sample. (For a complete description of the temperature gradients within the sample, see Caffrey et al., 1990). From an inspection of the data three distinct phases are apparent, each with its own characteristic I-2θ scan. The lower, mid, and upper section of the figure corresponds to the $L_{\beta'}$, $P_{\beta'}$, and L_α phases, respectively. The $L_{\beta'}$ to $P_{\beta'}$ transition is characterized by what appears to be a continuous shift in peak position from high to low angles (Figs. 2 and 3). At the same time peak intensity decreases considerably and the peak appears to broaden (Fig. 2). There is also a rise in the scattering intensity between the first and second order lamellar reflections as noted above.

At the $P_{\beta'}$ to L_α transition the sequence of events observed at the $L_{\beta'}$ to $P_{\beta'}$ transition is reversed. The low-angle (001) reflection sharpens and grows in intensity as it moves to higher angles and the level of scatter between the first two lamellar reflections drops. With continued heating in the L_α phase there is a gradual shift to higher angles of the low-angle (001) and (002) peaks corresponding to a fall in lamellar *d*-spacing.

We note that both the premelting ($L_{\beta'}$-$P_{\beta'}$) and the main transitions ($P_{\beta'}$-L_α) appear continuous based on the data presented in Figs. 2 and 3. At no point during either phase change is there evidence for a two-state coexistence. In such a case, low-angle reflections from both phases would be expected to be seen simultaneously during the transition. We emphasize, however, that the limited spatial resolution of our imaging/recording device and limited temperature resolution precludes a definitive statement in this regard. This is particularly evident for the $P_{\beta'}$ phase which has a rather complicated low-angle diffraction pattern with a multitude of strong and weak reflections in the region of interest. Naturally, the pattern becomes even more crowded in the region of phase coexistence.

Dynamic measurements

Studies of the kinetics and mechanism of the $L_{\beta'}$-$P_{\beta'}$-L_α transitions were performed by using microwave-induced temperature-jump perturbations. Temperature jumps of varying amplitudes provided for a range of sample heating rates and, of necessity, final sample temperatures. The transitions themselves were monitored by TRXRD exactly as described above under Equilibrium Measurements. The results are presented in Fig. 4 which shows the change in low-angle peak position, corresponding to inverse *d*-spacing, with time after temperature jumps of four distinct amplitudes and, thus, heating rate. A sampling of the original I-2θ scans recorded during a 120-W temperature jump is presented in Fig. 5. To enhance readability the data in Fig. 4 are presented with time on a log scale. The semi-log plot serves to contract the spread of data at long time intervals and to expand it at short times. Because measurements were made from the same initial room temperature value of ~27° C, every sample begins in the $L_{\beta'}$ phase. In all cases, the final microwave setting is sufficient to effect complete conversion to the L_α

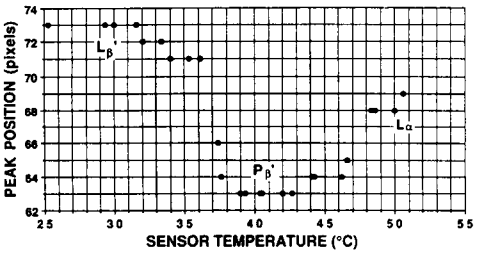

FIGURE 3 Thermal equilibrium measurements of the microwave-induced $L_{\beta'}$-$P_{\beta'}$-L_α phase transition sequence occurring in fully hydrated DPPC. Low-angle x-ray diffraction was recorded in live time and the strongest low-angle peak position was determined by image processing as described under Materials and Methods. Each data point corresponds to a single (33 ms) frame with radial averaging over a 20° arc. Measurements were made in the heating direction using a maximum microwave power setting of 7 W. Samples were incubated for 2 min at a given microwave power setting before TRXRD measurements were made. *It is important to note that the temperature shown on the abscissa is that recorded at the sensor and is not that at the position in the sample of the interrogating x-ray beam.*

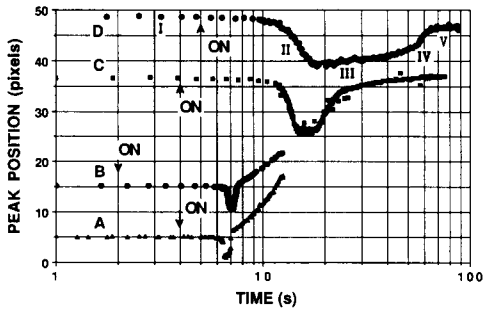

FIGURE 4 Kinetics of the $L_{\beta'}$-$P_{\beta'}$-L_α phase transitions in fully hydrated DPPC after a microwave-induced temperature jump. Final microwave power settings are 120 W (*A*), 100 W (*B*), 15 W (*C*), and 8 W (*D*). The position of the strongest low-angle peak maximum is plotted as a function of time before and after the application of the temperature jump (indicated by an arrow). For clarity, individual curves are displaced on the abscissa and ordinate and time is presented on a log scale. The five stages in the $L_{\beta'}$-$P_{\beta'}$-L_α transformation indicated in (*D*) are referred to in the text.

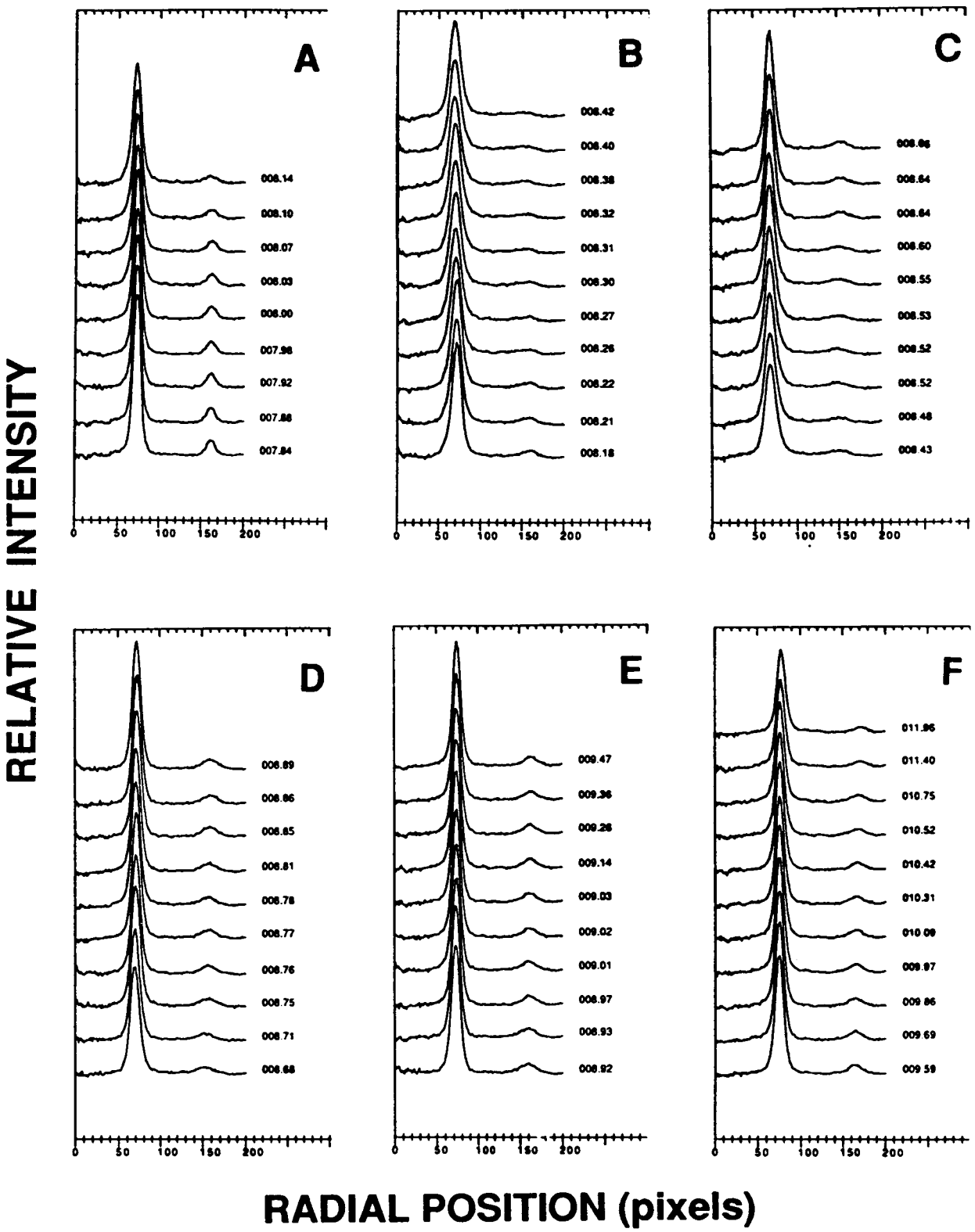

FIGURE 5 Kinetics of the $L_{\beta'}$-$P_{\beta'}$-L_{α} phase changes undergone by fully hydrated DPPC after a 120-W microwave-induced temperature jump. Experimental conditions are described under Materials and Methods. Elapsed time in seconds is indicated to the right hand side of each low-angle scan. Microwave power was turned on at ~8.1 s. Patterns typical of the $L_{\beta'}$, $P_{\beta'}$, and L_{α} phase are evident at 7.84, 8.31, and 9.03 s, respectively.

phase which, assuming no nonthermal microwave effects, corresponds to a sample temperature in excess of 42° C. At intermediate temperatures the $P_{\beta'}$ phase is in evidence.

The progress curves in Fig. 4 have five distinct regions identified as I–V in Fig. 4 *D* as follows. Region I is flat and corresponds to the pure $L_{\beta'}$ phase whose coefficient of thermal expansion is negligible. Region II represents the time interval in which the $L_{\beta'}$-to-$P_{\beta'}$ transformation takes place. Region III corresponds to the pure $P_{\beta'}$ phase undergoing a continuous decrease in lamellar *d*-spacing upon heating. Conversion from the $P_{\beta'}$ to L_α phase occurs in Region IV which is followed by Region V representing pure L_α phase undergoing heating.

As the temperature-jump amplitude and heating rate are adjusted we note the following changes in the response of the sample. To begin with, as rate increases so too does final sample temperature. This accounts for the difference in the relative heights of Regions I and V observed in the four plots in Fig. 4. The higher the low-angle peak position, and thus scattering angle, the smaller is the corresponding lamellar *d*-spacing which reflects the negative thermal expansion coefficient of the L_α phase.

The next most obvious effect of increasing heating rate is the diminution of Region III corresponding to the time interval in which the pure $P_{\beta'}$ phase is observed. However, regardless of the heating rate, up to the maximum obtained at a microwave power setting of 120 W, a low-angle diffraction pattern characteristic of the $P_{\beta'}$ phase was always observed at times intermediate between the loss of the $L_{\beta'}$ phase and the emergence of the L_α phase. This result shows that under current conditions it was not possible to bypass the $P_{\beta'}$ phase in temperature jumps from the $L_{\beta'}$ to the L_α phase in fully hydrated DPPC.

Another interesting feature to emerge from these temperature-jump experiments concerns the dependence of the degree of $P_{\beta'}$ phase development on heating rate. The degree of development is evaluated as the magnitude of the difference in peak position (ΔP) between the stable $L_{\beta'}$ and the transient $P_{\beta'}$ phase. The equilibrium measurements show a maximum ΔP value of ~10 pixels (Fig. 3). Using 8- and 15-W power settings in the kinetic measurements this same equilibrium ΔP value is observed. However, at the higher heating rates associated with the 100- and 120-W power settings ΔP values of 4.5 and 4 pixels, respectively, are observed. This corresponds to a smaller *d*-spacing in the $P_{\beta'}$ phase than was found under equilibrium and slow heating conditions.

In all cases, with the exception of the 120-W temperature jump, samples were allowed to reach an equilibrium final temperature as dictated by the particular microwave power setting. In the latter case, temperature rose to above 100° C and resulted in water boiling off the exposed sample. The data presented in Fig. 4 *A*, therefore, cover the range up to but not including the high temperature domain.

As was observed under Equilibrium Measurements, the kinetic data suggest, to within the sensitivity limits of our detection/recording device, that both the premelting and main transitions are continuous rather than two state. Further, because of the limited angular resolution available and the complex nature of the $P_{\beta'}$ phase diffraction pattern, we cannot address conclusively the issue of the possible appearance of intermediates in the transition process. We can say, however, that if such intermediates exist they appear in the vicinity of the $L_{\beta'}$, $P_{\beta'}$, or L_α phase low-angle reflections and/or are of low frequency without significant accumulation during the transition.

Because the focus of this study is the dynamics and mechanism of the heat-driven phase changes only brief mention will be made of the L_α to $P_{\beta'}$ cooling transition. Sample data from the 15-W heating experiment are shown in Fig. 6. In this experiment, cooling into the $P_{\beta'}$ phase alone was monitored. Conversion to the $L_{\beta'}$ phase was not followed because of the slowness of the transition. Upon cooling we see that the peak position of the (001) reflection of the L_α phase drops continuously with time after microwave radiation is turned off. The onset of the actual L_α to $P_{\beta'}$ transition is signalled by a small, transient increase in peak position after which peak position continues to decrease and eventually settles at a value characteristic of the fully developed $P_{\beta'}$ phase. We attribute the latter, short-lived increase in peak position to sample warming brought about by the latent heat of the transi-

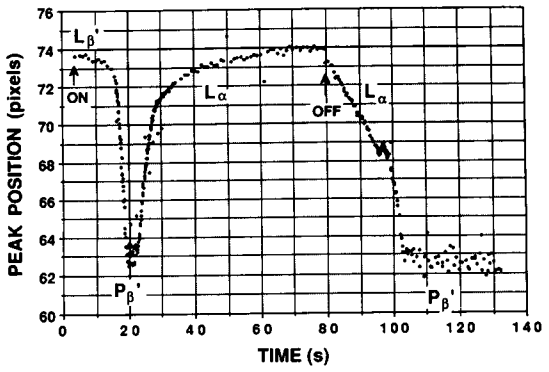

FIGURE 6 Kinetics of the $L_{\beta'}$-$P_{\beta'}$-L_α phase transitions undergone by fully hydrated DPPC in response to a 15-W microwave-induced temperature jump and subsequent passive cooling. Measurements were made as described in the legend to Fig. 4. The point in time when microwave radiation was turned on and off is so indicated.

tion ($\Delta H \simeq$ 8.7 kcal/mol, Mabrey and Sturtevant, 1976). This has the effect of elevating peak position, reflecting the pronounced thermal expansion coefficient of the residual L_α phase in the transition region. This same behavior was observed in a number of the other cooling progress curves (data not shown).

DISCUSSION

The results show clearly that with the maximum heating rate employed in these experiments it was not possible to induce a direct $L_{\beta'}$ to L_α transition in fully hydrated DPPC. At all heating rates, a $P_{\beta'}$ phase appeared as an intermediate in the thermotropic process. Under equilibrium conditions the $P_{\beta'}$ phase is found as an intermediate phase sandwiched between the two lamellar phases, $L_{\beta'}$ and L_α. In this study, we attempted a direct $L_{\beta'}$ to L_α phase transition by rapid heating. By all appearances, up to the maximum heating rate used, equilibrium-type behavior is followed in these kinetic experiments. The results do not preclude the possibility that with even faster heating the $P_{\beta'}$ phase can be bypassed. We did find, however, that at the faster heating rates the development of the $P_{\beta'}$ phase was less complete. This was evidenced by a failure of the evolving $P_{\beta'}$ phase to realize a lamellar repeat size characteristic of that observed under equilibrium conditions or at the lower heating rates.

The transit times of the pre- and chain-melting transitions occurring in fully hydrated DPPC have been determined based on the TRXRD measurements. These are assembled in Table 1. The data show that as microwave power and, thus, heating rate increases, the corresponding heating transit times decrease. This result suggests that higher incident microwave power will be required to establish the limiting transit times in each case. At the fastest heating rate used in these experiments, corresponding to a microwave power setting of 120 W, the $L_{\beta'}$-$P_{\beta'}$-L_α transition sequence was complete in <1 s. It is important to realize that this transit time includes the time required to raise sample temperature through the 5–7° C range in which the $P_{\beta'}$ phase is stable. Thus, the intrinsic transit times for the individual $L_{\beta'}$ to $P_{\beta'}$ and $P_{\beta'}$ to L_α transitions are of order 100 ms or less (see Fig. 5, for example). The L_α to $P_{\beta'}$ cooling transition which was examined in a passive cooling mode by contrast has a transit time of many seconds.

Careful slow-scan TRXRD and high sensitivity differential scanning calorimetry and AC calorimetric measurements carried out by Tenchov et al. (1989) reveal a new metastable $P_{\beta'}$ ($P_{\beta'}$ mst) phase occurring in fully hydrated DPPC. The latter is obtained by cooling from the L_α phase to a temperature intermediate between the pre- and main transition temperatures. The original $P_{\beta'}$ phase can be recovered by first quenching the sample into the $L_{\beta'}$ phase and reheating through the pretransition. The $P_{\beta'}$ (mst) has a characteristic low-angle diffraction pattern (see Fig. 7 *G*) and possesses a higher heat content compared with $P_{\beta'}$. The latter is reflected in the 5% lower enthalpy change at the $P_{\beta'}$ (mst) to L_α transition compared with the $P_{\beta'}$ to L_α transition. As described by Tenchov et al. (1989) the "$P_{\beta'}$ (mst) should not be considered as less solid than $P_{\beta'}$ but rather less ordered with respect to correlations and stacking between bilayers."

In contrast to the results of Tenchov et al. (1989) we do not find a big difference in the low-angle diffraction pattern of the $P_{\beta'}$ phase obtained upon heating from $L_{\beta'}$ or cooling from the L_α phase (Fig. 7). To what can we ascribe this apparent difference in behavior? To begin with, the lipid used by Tenchov et al. (1989) was dispersed in deionized water (pH 5.3, conductivity <2 μS) while we used a Hepes/NaCl/KCl buffer, pH 7.4. Extremely slow heating and cooling scan rates of 0.1° C/min were used by Tenchov et al. (1989) while we used relatively rapid, active heating, and passive cooling. In our experiments the lipid had been exposed to microwave

TABLE 1 Transit times of the thermotropic phase transitions undergone by fully hydrated DPPC in response to microwave-induced temperature-jumps*

	Transit time‡ (*s*)			
	Heat			Cool
Microwave power	$L_{\beta'} \rightarrow P_{\beta'}$	$P_{\beta'} \rightarrow L_\alpha$	$L_{\beta'} \rightarrow P_{\beta'} \rightarrow L_\alpha$	$L_\alpha \rightarrow P_{\beta'}$
W				
8	5	15	38	—
15	2	3	20	8
100	—	—	1	10
120	—	—	<1	—

*Progress of the transition was monitored by low-angle time-resolved x-ray diffraction.

‡Transit time refers to the time it takes to undergo the indicated phase change as judged by visual inspection of the video-recorded TRXRD images. Transit time is the time interval between the first sighting of diffraction from the newly forming phase and the last detectable diffraction from the phase undergoing the transformation. Due to the congested nature of the $P_{\beta'}$ phase diffraction pattern, it was normally not possible to accurately determine when the phase undergoing the transition had finally disappeared. Our criterion for completion of the transition was thus the point in time where a change in the scattering behavior of the newly formed $P_{\beta'}$ phase could not be discerned. The transit times reported are gross values and include the time required to (*a*) heat/cool the sample through the transition temperature range, (*b*) supply/remove the latent heat of the transition, and (*c*) undergo the transition, i.e., the intrinsic or net transit time. Thus, the intrinsic time is always less than the measured gross value.

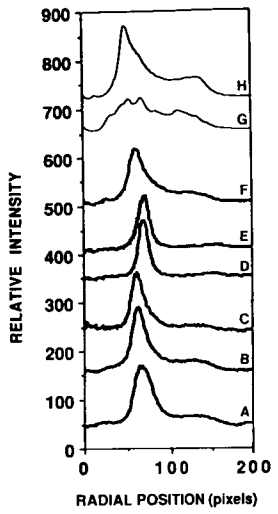

FIGURE 7 Low-angle x-ray diffraction from the $P_{\beta'}$ phase of fully hydrated DPPC under a variety of heating and cooling conditions. Scans *A–F* were recorded during the course of the present study. Scans *G* and *H* are tracings from Fig. 4 in the paper by Tenchov et al. (1989) and correspond to the $P_{\beta'}$ (mst) and $P_{\beta'}$ phases, respectively. Scan *A* corresponds to the $P_{\beta'}$ phase observed at 37.4°C during the equilibrium heating measurements reported in Fig. 3. Scans *B–E* correspond to the $P_{\beta'}$ phase observed during temperature jump heating and were recorded using microwave power settings of 8, 15, 100, and 120 W, respectively. Scan *F* was obtained upon cooling from the L_α phase after a temperature jump in which a microwave power setting of 13 W was used. The scan was obtained 54 s after the microwave power had been turned off and corresponds to a point in time when the $P_{\beta'}$ phase was "fully developed."

radiation before cooling into the $P_{\beta'}$ phase. In contrast, Tenchov et al. (1989) used a temperature regulated water stream to control sample temperature. Of these differences, the ones most likely to contribute to a disparate behavior upon cooling include heating and cooling rates and the fact that microwaves were used in our experiments. We note, however, that in the cooling direction where the differences arise microwave radiation was not imposed on the sample. Thus, if the microwave effect is important, it must be long-lived, persisting after the microwaves had been turned off. We consider this an unlikely possiblity. Thus, we are left with the rate of cooling as a potential source of disparate behavior. Perhaps the relatively rapid cooling used in our experiments is such as to induce $P_{\beta'}$ phase formation. Slow cooling, on the other hand, may not provide a sufficiently large driving force initially upon $P_{\beta'}$ phase formation to facilitate the formation of the fully developed, correlated rippled condition characteristic of the $P_{\beta'}$ phase.

We thank B. W. Batterman (National Science Foundation, grant DMR 81-12822) and the entire CHESS and MacCHESS (National Institutes of Health, grant RR-014646) staff for their invaluable help and support. The assistance of A. P. Mencke with image processing and data analysis is gratefully acknowledged. Valuable comments on this manuscript were provided by Dr. B. Tenchov.

This work was supported by a grant from the National Institutes of Health (DK 36849) and by a University Exploratory Research Program (The Procter and Gamble Co.) and a Du Pont Young Faculty award to M. Caffrey.

Received for publication 5 February 1990 and in final form 30 April 1990.

REFERENCES

Blume, A., and M. Hillmann. 1986. Dimyristoylphosphatidic acid/cholesterol bilayers: thermodynamic properties and kinetics of the phase transition as studied by the pressure jump relaxation technique. *Eur. Biophys. J.* 13:343–353.

Caffrey, M. 1984*a*. Kinetics and mechanism of the lamellar gel/lamellar liquid crystal and lamellar/inverted hexagonal phase transition in phosphatidylethanolamine: a real-time x-ray diffraction study using synchrotron radiation. *Biochemistry.* 24:4826–4844.

Caffrey, M. 1984*b*. X-Radiation damage of hydrated lecithin membranes detected by real-time x-ray diffraction using wiggler-enhanced synchrotron radiation as the ionizing radiation source. *Nucl. Instr. Meth.* 222:329–338.

Caffrey, M. 1987. Kinetics and mechanism of transitions involving the lamellar, cubic, inverted hexagonal and fluid isotropic phase of hydrated monoacylglycerides monitored by time-resolved x-ray diffraction. *Biochemistry.* 26:6349–6363.

Caffrey, M. 1989*a*. The study of lipid phase transition kinetics by time-resolved x-ray diffraction. *Annu. Rev. Biophys. Biophys. Chem.* 18:159–186.

Caffrey, M. 1989*b*. Structural, mesomorphic and time-resolved studies of biological liquid crystals and lipid membranes using synchrotron radiation. *Top. Curr. Chem.* 151:75–109.

Caffrey, M., and G. W. Feigenson. 1981. Fluorescence quenching in model membranes: the relationship between Ca^{2+}-ATPase enzyme activity and the affinity of the protein for phosphatidylcholines with different acyl chain characteristics. *Biochemistry.* 20:1949–1961.

Caffrey, M., and D. H. Bilderback. 1984. Kinetics of the main phase transition of hydrated lecithin monitored by real-time x-ray diffraction. *Biophys. J.* 45:627–631.

Caffrey, M., and G. W. Feigenson. 1984. The influence of metal ions on the phase properties of phosphatidic acid in combination with natural and synthetic phosphatidylcholines: an x-ray diffraction study using synchrotron radiation. *Biochemistry.* 23:323–331.

Caffrey, M., R. L. Magin, B. Hummel, and J. Zhang. 1990. Kinetics of the lamellar and hexagonal phase transitions in phosphatidylethanolamine: a time-resolved x-ray diffraction study using a microwave-induced temperature-jump. *Biophys. J.* 58:21–29.

Cho, K. C., C. L. Choy, and R. Young. 1981. Kinetics of the pretransition of synthetic phospholipids: a calorimetric study. *Biochim. Biophys. Acta.* 663:14–21.

Genz, A., and J. F. Holzwarth. 1986. Dynamic flourescence measurements on the main phase transition of dipalmitoylphosphatidylcholine vesicles. *Eur. Biophys. J.* 13:323–330.

Genz, A., J. F. Holzwarth, and T. Y. Tsong. 1986. The influence of cholesterol on the main phase transition of unilamellar dipalmi-

toylphosphatidylcholine vesicles: a differential scanning calorimetry and iodine laser T-jump study. *Biophys. J.* 50:1043–1051.

Inoko, Y., T. Mitsui, K. Ohki, T. Sekiya, and Y. Nozawa. 1980. X-Ray and electron microscopic studies of the undulated phase in lipid/water systems. *Phys. Stat. Sol. a.* 60:115–121.

Inoue, S., M. Nishimura, and T. Yasunaga. 1981. Studies on the phase transition in the single lamellar liposomes. 3. Kinetic behavior of the phase transition. *J. Phys. Chem.* 85:1401–1405.

Inoue, T., H. Ohshima, H. Kamaya, and I. Ueda. 1985. Stopped-flow rapid kinetics of anesthetic-induced phase transition in phospholipid vesicle membranes: nonlocalized fluctuations. *Biochim. Biophys. Acta.* 818:117–122.

Janiak, M. J., D. M. Small, and G. G. Shipley. 1976. Nature of the thermal pretransition of synthetic phospholipids: dimyristoyl- and dipalmitoyllecithin. *Biochemistry.* 15:4575–4580.

Johnson, M. J., T. C. Winter, and R. L. Biltonen. 1983. The measurement of the kinetics of lipid phase transitions: a volume-perturbation kinetic calorimeter. *Anal. Biochem.* 128:1–6.

Lentz, B. R., E. Freire, and R. L. Biltonen. 1978. Flourescence and calorimetric studies of phase transitions in phosphatidylcholine multilayers: kinetics of the pretransition. *Biochemistry.* 17:4475–4480.

Luzzati, V. 1968. X-ray diffraction studies of lipid-water systems. *In* Biological Membranes, Physical Fact and Function. D. Chapman, editor. Academic Press, New York. 1:71–123.

Mabrey, S., and J. M. Sturtevant. 1976. Investigation of phase transitions of lipids and lipid mixtures by high sensitivity differential scanning calorimetry. *Proc. Natl. Acad. Sci. USA.* 73:3862–3866.

Mayorga, O. L., J. L. Lacomba, and E. Freire. 1988. Multifrequency calorimetry of phospholipid bilayer membranes. *Biophys. J.* 53:125*a*. (Abstr.)

Shashidar, R., B. P. Gaber, S. K. Prasna, and S. Chandrasekhar. 1984. High pressure study of phase transitions in DMPC-water system. *Mol. Cryst. Liq. Cryst.* 110:153–160.

Small, D. M. 1987. Handbook of lipid research: the physical chemistry of lipids from alkanes to phospholipids. Plenum Publishing Corporation. New York. 4:672 pp.

Subczynski, W. K., and A. Kusumi. 1986. Effects of very small amounts of cholesterol on gel-phase phosphatidylcholine membranes. *Biochim. Biophys. Acta.* 854:318–320.

Teissie, J. 1979. Fluorescence temperature jump relaxations of dansylphosphatidylethanolamine in aqueous dispersions of dipalmitoylphosphatidylcholine during the gel to liquid-crystal transition. *Biochim. Biophys. Acta.* 555:553–557.

Tenchov, B. G., H. Yao, and I. Hatta. 1989. Time-resolved x-ray diffraction and calorimetric studies at low scan rates. *Biophys. J.* 56:757–768.

Tsong, T. Y. 1974. Kinetics of the crystalline-liquid crystalline phase transition of dimyristoyl L-α-lecithin bilayers. *Proc. Natl. Acad. Sci. USA.* 71:2684–2688.

Tsong, T. Y., and M. I. Kanehisa. 1977. Relaxation phenomena in aqueous dispersions of synthetic lecithins. *Biochemistry.* 16:2674–2680.

Tsuchida, K., I. Hatta, S. Imaizumi, K. Ohki, and Y. Nozawa. 1985. Kinetics near the pretransition of a multilamellar phospholipid studied by ESR. *Biochim. Biophys. Acta.* 812:249–254.

Wack, D. C., and W. W. Webb. 1989. Synchrotron x-ray study of the modulated lamellar phase $P_{\beta'}$ in the lecithin-water system. *Phys. Rev. A.* 40:2712–2730.

Wickersheim, K. A., and R. B. Alves. 1979. Recent advances in optical temperature measurement. *Industrial Research and Development.* 21:82–89.